ACS OMEGA

Open Access

http://pubs.acs.org/journal/acsodf

Article

Enhancing Dielectric Properties of ($CaCu_3Ti_4O_{12}$ NWs−Graphene)/PVDF Ternary Oriented Composites by Hot Stretching

Wenning Qi, Liuyang Li, Ruolin Han, Yanbin Hou, Zheng Zhou, Guang-Xin Chen,* and Qifang Li*

Cite This: *ACS Omega* 2024, 9, 13298−13305

Read Online

ACCESS | Metrics & More | Article Recommendations | Supporting Information

ABSTRACT: Using high-dielectric inorganic ceramics as fillers can effectively increase the dielectric constant of polymer-based composites. However, a high percentage of fillers will inevitably lead to a decrease in the mechanical toughness of the composite materials. By introducing high aspect ratio copper calcium titanate ($CaCu_3Ti_4O_{12}$) nanowires (CCTO NWs) and graphene as fillers, the ternary poly(vinylidene fluoride) (PVDF)-based composites (CCTO NWs−graphene)/PVDF with a significant one-dimensional orientation structure were prepared by hot stretching. CCTO NWs and graphene are arranged in a directional manner to form a large number of microcapacitor structures, which significantly improves the dielectric constant of the composites. When the ratio of CCTO NWs and graphene is 0.2 and 0.02, the oriented composites have the highest dielectric constant, which is 19.3% higher than the random composites, respectively. Numerical simulations reveal that the introduction of graphene and the construction of the one-dimensional oriented microstructure have a positive effect on improving the dielectric properties of the composites. This study provides a strategy to improve the dielectric properties of composite materials by structural design without changing the filler content, which has broad application prospects in the field of electronic devices.

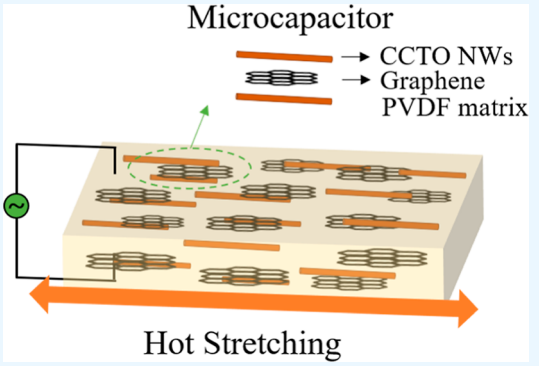

1. INTRODUCTION

Polymer-based dielectric materials have been widely used in electrostatic capacitors,[1,2] sensors,[3,4] pulse power systems,[5,6] and other fields due to their high dielectric properties, good processability, flexibility, and lightweight. For most organic polymers, the dielectric constant is less than 10. Therefore, the preparation of nanofillers/polymer composites has become an effective way to further improve the dielectric properties.[7] At present, the commonly used ceramic fillers include barium titanate (BT),[8−10] titanium dioxide (TiO_2),[11−13] and barium strontium titanate.[14,15] In addition, these ceramic nanoparticles can be transformed into one-dimensional nanowires or two-dimensional nanosheets to further improve the dielectric properties of the ceramic-filled composites.[16,17] Many studies have shown that one-dimensional ceramic fillers with high aspect ratios have greater advantages than spherical ceramic fillers in enhancing the dielectric constant of composites with low filler addition. However, regardless of what dimension of ceramic nanofillers is used, the dielectric constant of composites can be improved only when the high ceramic filling amount is greater than 50%, which often leads to the destruction of mechanical properties of composites. Conductive nanofillers/polymer composites improve the dielectric properties by regulating the seepage network of the conductive nanofillers. This is usually considered to be two reasons: one is the interfacial polarization between the filler with the polymer matrix and the other is the increase in the effective electrode surface area caused by the interconnection of nanofiller clusters near the percolation threshold. The commonly used conductive nanofillers include metals (silver,[18] copper,[19] aluminum,[20] etc.), carbon materials [graphene,[21] single/multiwalled carbon nanotubes (CNTs),[22] carbon fibers,[23] etc.], and conductive polymers (polyaniline,[24] polypyrrole,[25] etc.). However, a high dielectric loss and an uncontrollable percolation threshold have become the biggest problems that limit the development and application of conductive nanofillers/polymer composites. In order to make up for the above shortcomings as much as possible, researchers have explored a series of three-phase composites by adding conductive fillers and inorganic ceramic fillers to the polymer matrix.[26−28]

Researchers often use filler surface modification and macroscopic structure design to further improve the performance of three-phase polymer-based dielectric materials. By designing the coating layer microstructure of the nanofillers, we can effectively improve the dispersion and compatibility of the nanofillers in the polymer matrix, and the internal defects

Received: December 18, 2023
Revised: February 23, 2024
Accepted: February 28, 2024
Published: March 7, 2024

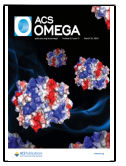

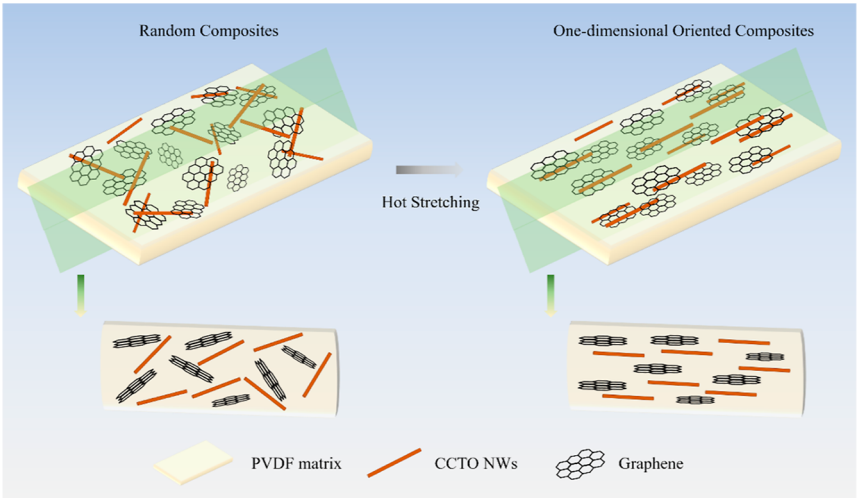

Figure 1. Processing flow diagram of ternary (CCTO NWs−graphene)/PVDF composites with random/oriented structures.

of the composites can be reduced. In addition, it can also reduce the adverse effects caused by the difference in electrical properties between the filling phase and the matrix. Starting from the structural design of composite materials, researchers have prepared orientation structures, sandwich structures,[29−31] multilayer gradient structures,[32−34] three-dimensional network structures,[35−38] etc. Song[39] et al. prepared Bi_2S_3/BT/poly(vinylidene difluoride) (PVDF) composites with significant orientation structure by hot stretching, and their dielectric properties are consistent with those of parallel microcapacitors. Feng[40] et al. used Ti_3C_2 and hexagonal boron nitride as fillers to prepare PVDF-based composites with sandwich structures and excellent dielectric properties at high temperatures. Ma[4] et al. coated CNTs/BT colloids on the polyurethane foam as the three-dimensional skeleton and prepared a foam-based flexible capacitive sensor with a wide response range. These findings fully demonstrate that the design and establishment of the composites' macroscopic structure can effectively improve their dielectric properties.

Here, we synthesized copper calcium titanate ($CaCu_3Ti_4O_{12}$) nanowires (CCTO NWs) with a high aspect ratio by a two-step hydrothermal method and introduced a small amount of graphene as the second filler, and then a novel oriented ternary (CCTO NWs−graphene)/PVDF composite architecture was constructed via a hot stretching process. Under the action of external force, CCTO NWs and graphene are aligned to form numerous microcapacitor structures, which endows three-phase polymer-based orientation composites with high dielectric constant and low dielectric loss. At the same time, the low filler content (only 22% of the PVDF matrix mass) maintains excellent mechanical properties of the polymer-based dielectric materials.

2. EXPERIMENTAL SECTION

2.1. Materials. TiO_2 nanopowder and copper nitrate trihydrate [$Cu(NO_3)_2{\cdot}3H_2O$] were purchased from Aladdin. Calcium acetate monohydrate [$Ca(CH_3COO)_2{\cdot}H_2O$] was purchased from Innochem. γ-Aminopropyl-triethoxysilane (KH550) was bought from J&K Chemicals. *N*,*N*-Dimethylformamide (DMF) was supplied by Beijing Tongguang Fine Chemical Company. Graphene slurry was provided by MORSH. PVDF was purchased from Kureha Chemical, Japan. All the chemicals were of analytical grade and used without further purification.

2.2. Fabrication of Oriented Ternary (CCTO NWs−Graphene)/PVDF Composites. The synthesis of CCTO NWs was performed through a two-step hydrothermal reaction, details of which can be obtained from our earlier reported work.[41,42] The related performance tests are shown in Figures S1 and S2. Figure 1 shows the processing flow diagram of ternary (CCTO NWs−graphene)/PVDF composites with random/oriented structures. In order to facilitate the weighing and calculation, the composite materials were named in the form of proportions. When the mass of the matrix was 1 g, the mass of CCTO NWs was *x*, and the mass of graphene was *y*, it was named (*x*CCTO NWs−*y*graphene)/PVDF. In this experiment, the ternary composites were designed with the CCTO NWs content fixed at 0.2 and changing the content of graphene from 0 to 0.02. Before fillers were incorporated into PVDF, CCTO NWs were modified by mixing with 1 wt % KH550 in ethanol (Figure S3). First, a certain mass of graphene slurry was added to 15 mL of DMF solvent and ultrasonically peeled for 4 h to form a uniform graphene mixed solution (Figures S4 and S5), and then PVDF pellets were added to it to form a uniform suspension A, heated, and stirred at 70 °C. A certain mass of CCTO NWs was added in DMF solvent and ultrasonically peeled for 30 min to obtain mixed solution B. A and B were mixed, stirred, and ultrasonically dispersed for 1 h to prevent the agglomeration of CCTO NWs and graphene. The mixed solution was then heated at 80 °C to remove the excess solvent. The dried product was placed in a mold and hot-pressed at 180 °C to obtain random ternary composites. The oriented ternary composites were prepared by a simple thermal stretching process. First, the samples were placed on a 160 °C hot press, and a certain pressure was applied to fix them. The samples were uniaxially stretched in the horizontal direction. The stretched samples were placed into the mold along the direction of the tensile force, recompressed at 180 °C, and then continued to be stretched along the tensile direction at 160 °C. This process was repeated 4 times. Finally, the ternary composites with random/oriented structures and different filler contents were prepared, which were named (0.2CCTO NWs−*y*graphene)/PVDF (*y* = 0, 0.0025, 0.005, 0.0075, 0.01, and 0.02).

https://doi.org/10.1021/acsomega.3c10111
ACS Omega 2024, 9, 13298−13305

2.3. Characterization. The morphology of CCTO NWs and the cross-sectional microstructures of ternary composites were observed through scanning electron microscopy (SEM, MAIA3 TESCAN). The remaining microstructures were obtained using a transmission electron microscope (FEI Tecnai G2 F20 460L) at an acceleration voltage of 300 kV. Dielectric properties were measured by an Agilent 4294A with a 16451B fixture, in the frequency range from 40 to 30 MHz at room temperature. The crystalline structure and phase morphology of the filler and nanocomposites were characterized by an X-ray diffraction (XRD) instrument (ESCALAB 250). Differential scanning calorimetry (DSC, NETZSCH 203) was carried out under a nitrogen atmosphere to measure the phase change of the composite before and after stretching. The chemical structure of samples was analyzed by Fourier transform infrared (FTIR) spectroscopy (Bruker Tensor-27) in the range of 500−4000 cm^{-1}. Raman spectra were recorded at room temperature on a LABRAM-010 confocal laser micro-Raman spectrometer (Jobin Yvon).

2.4. Finite-Element Simulation. The electric field and electric displacement vector of binary/ternary composites with random/oriented structures were simulated by two-dimensional models established by the finite-element method. A series of clear two-dimensional idealized models were established to simulate the electric field and the electric displacement vector of binary/ternary composites with random/oriented structures. The CCTO NWs were set as 10 rectangular regions (length: 10 μm; width: 0.3 μm), and the relative dielectric constant was 10^5. The graphene sheets were set as 25 rectangular regions (length: 6 μm; width: 0.1 μm), and the relative dielectric constant was 10^9. PVDF was set to a continuous rectangular area (length: 50 μm; width: 30 μm), and the relative dielectric constant was 10. For the remaining parameters, one can refer to the material library data. A voltage of 300 V was applied in the vertical direction of the composite model.

3. RESULTS AND DISCUSSION

As presented in the cross-sectional SEM images of oriented xCCTO NWs/PVDF composites (x = 0.1, 0.2, 0.3, and 0.4) (Figure 2a−d), the CCTO NWs are aligned along the direction of the external force. This indicates that when the PVDF is in a semimolten state, a uniaxial tensile force can be applied to the composite material to cause the movement of the filler in the microscopic state so that the CCTO NWs are oriented along the direction of the tensile force. When the additional amount of CCTO NWs is increased from 0.1 to 0.4, the spacing between CCTO NWs becomes more minor, but the overall arrangement is still in the direction of tension. The system has no apparent agglomerations and defects, showing good compatibility. This is mainly due to the interaction of small molecular groups on the surface of CCTO NWs, which prevents the mutual contact between CCTO NWs.

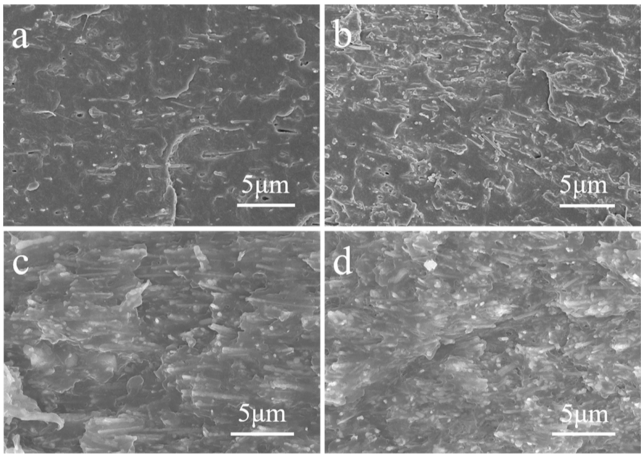

Figure 2. Cross-sectional SEM images of oriented (a) 0.1CCTO NWs/PVDF, (b) 0.2CCTO NWs/PVDF, (c) 0.3CCTO NWs/PVDF, and (d) 0.4CCTO NWs/PVDF composites.

Figure 3 shows the cross-sectional SEM images and microstructure diagram of the oriented (0.2CCTO NWs−$y$graphene)/PVDF composites (y = 0.005, 0.01, and 0.02) with graphene content increasing. As shown in Figure 3a−c, both the CCTO NWs and graphene are aligned along the direction of the external force. Graphene exhibits a directional layer-by-layer distribution in the stretching direction, and CCTO NWs are also uniformly dispersed between graphene, forming a graphene−CCTO NWs−graphene like a microcapacitor structure. As the amount of conductive filler increases from 0.005 to 0.02, the layer-by-layer parallel distribution of graphene sheets becomes more apparent. The spacing between the graphene sheets gradually becomes smaller, and the overlapping area of the sheets increases, which is beneficial to improving the microcapacitors' performance. This significant change in microstructure can be clearly seen in Figure 3d.

Applying uniaxial tensile strain will change the polymer matrix's molecular structure and the fillers' distribution. The material's structural anisotropy due to the macroscopic stress will cause the anisotropy of the material's dielectric properties. Dielectric properties perpendicular to the tensile direction of the prepared xCCTO NWs/PVDF composites (x = 0, 0.1, 0.2, 0.3, and 0.4) and $y$graphene/PVDF composites (y = 0, 0.0025, 0.005, 0.0075, 0.01, and 0.02) were tested, and the optimal ratio of these two fillers was determined. The relevant data obtained from the test are clearly shown in Figure 4a−d and Tables S1 and S2. CCTO NWs with a high aspect ratio have a higher dipole moment and dielectric constant, so the dielectric constant of the composites increases with the increase of the CCTO NWs ratio. At the same CCTO NWs ratio, the dielectric constant of the oriented composites is slightly lower than that of the random composites (Figure 4a). This phenomenon may be connected with the reason that the random composites possess a stronger dipole polarization in the through-plane direction in the direction perpendicular to the electric field, and the directional arrangement of CCTO NWs caused by thermal stretching reduces the polarization of the composites.[43] It can be seen from Figure 4b that the dielectric loss of the composites at 1 kHz is not more than 0.05, which is at a low level. This can be explained by the low amount of CCTO NWs added, and the surface modification of KH550 makes fillers and the matrix have good compatibility. The dielectric loss of the oriented composites is slightly lower than that of the random composites, which is mainly because the directional arrangement of the CCTO NWs reduces the polarization of the system and the dielectric loss. At 1 kHz (Table S1), when the CCTO NWs ratio is less than 0.3, the dielectric loss value of the composites is lower than that of pure PVDF, which is because the addition of CCTO NWs reduces the number of dipoles in PVDF. When the CCTO NWs ratio exceeds 0.3, the dielectric loss caused by CCTO

https://doi.org/10.1021/acsomega.3c10111
ACS Omega 2024, 9, 13298−13305

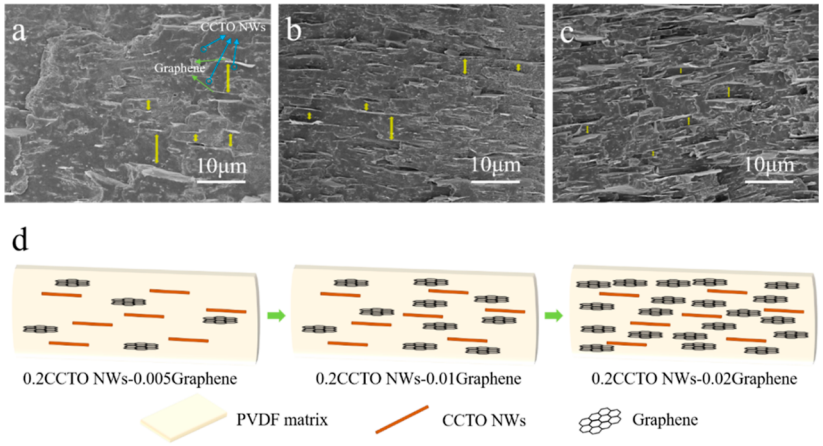

Figure 3. Cross-sectional SEM images of oriented (a) (0.2CCTO NWs−0.005graphene)/PVDF composites, (b) (0.2CCTO NWs−0.01graphene)/PVDF composites, and (c) (0.2CCTO NWs−0.02graphene)/PVDF composites. (d) Microstructure diagram of the ternary oriented composites with graphene content increasing.

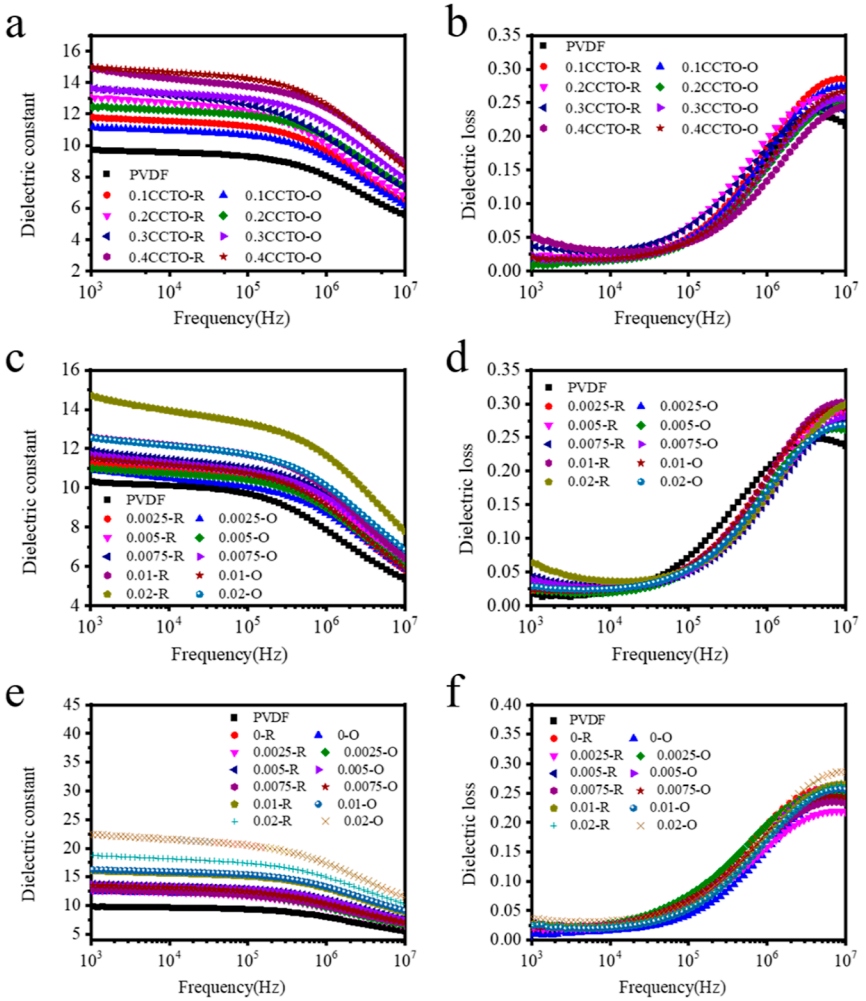

Figure 4. (a) Dielectric constant and (b) dielectric loss of *x*CCTO NWs/PVDF composites (x = 0, 0.1, 0.2, 0.3, and 0.4). (c) Dielectric constant and (d) dielectric loss of *y*graphene/PVDF composites (y = 0, 0.0025, 0.005, 0.0075, 0.01, and 0.02). (e) Dielectric constant and (f) dielectric loss of (*x*CCTO NWs−*y*graphene)/PVDF composites (x = 0, 0.2; y = 0, 0.0025, 0.005, 0.0075, 0.01, and 0.02).

NWs is higher than that caused by PVDF dipole reduction, so the dielectric loss of the composites increases.

Graphene nanosheets have an extremely high specific surface area and electrical conductivity. Therefore, a small amount of graphene can be used to composite with the PVDF matrix to effectively improve the dielectric constant of the composites effectively. However, the low percolation threshold of graphene often leads to a high dielectric loss. It can be seen from Figure 4c,d that when the amount of graphene added is less than 0.02, it has little effect on the dielectric constant of graphene/PVDF

https://doi.org/10.1021/acsomega.3c10111
ACS Omega 2024, 9, 13298−13305

binary random composites, and all samples have a dielectric loss value of less than 0.05. With the increase of graphene content to 0.02, the dielectric constant and dielectric loss of the binary random composites at 1 kHz increased to 14.69 and 0.063, respectively. The graphene content did not reach the percolation threshold of the system. Similarly, the dielectric constant of graphene/PVDF binary oriented composites also increases with the increase in the graphene content. The improvement of the dielectric constant is mainly related to successful microstructure construction. The graphene nanosheets are dispersed in parallel in the PVDF matrix, and a large number of graphene−PVDF−graphene layered structures are formed inside the oriented composites, which is similar to the nanocapacitor structure. With the increase in graphene content, the number of nanocapacitors also increases, and each nanocapacitor structure contributes to the final dielectric properties of the composites. Comparing the dielectric properties of random and oriented composites at 1 kHz (Table S2), it can be found that the dielectric constant of oriented composites is slightly lower than that of random composites at the same graphene ratio. Taking 0.02graphene/PVDF composites as an example, the dielectric constant value decreased from 14.69 to 12.55 and the dielectric loss value decreased from 0.063 to 0.029 after thermal tensile orientation treatment. The reason for this phenomenon can be explained by seepage theory. During the hot tensile orientation process, the agglomerated graphene nanosheets are dispersed and the conductive pathways inside the material are destroyed, which leads to a slight decrease in the dielectric constant of the oriented composites. The parallel arrangement of graphene nanosheets suppresses the leakage current in the system; therefore, the dielectric loss of the composites is significantly reduced.

The frequency dependence of the dielectric constant and dielectric loss of (xCCTO NWs−$y$graphene)/PVDF composites (x = 0 and 0.2; y = 0, 0.0025, 0.005, 0.0075, 0.01, and 0.02) are shown in Figure 4e,f. It can be observed that as the graphene ratio increases, the dielectric constant of the ternary composites shows a gentle trend. When the graphene ratio is 0.02, the dielectric constant has a particularly significant increase. The dielectric loss of ternary composites is maintained at a low level (less than 0.05 at 1 kHz). It can be clearly seen that the dielectric constant of the unoriented (0.2CCTO−0.02graphene)/PVDF composites is 143.6% of the 0.2CCTO/PVDF composites and even 125.6% of the 0.4CCTO/PVDF composites. Similarly, the dielectric constants of (0.2CCTO−0.02graphene)/PVDF oriented composites are 179.4 and 149.3% of the corresponding samples. To more intuitively understand the changes in the dielectric properties of the composites before and after thermal stretching, the dielectric constant and dielectric loss values at 1 kHz were analyzed (Table S3). The orientation of CCTO NWs and graphene in the direction perpendicular to the electric field causes the oriented composites to have a higher dielectric constant and a lower dielectric loss than the random composites. The oriented arrangement of graphene and CCTO NWs forms a large number of graphene−CCTO NWs−graphene and graphene−PVDF−graphene layered structures, which are similar to many microcapacitors in series and parallel, so the dielectric constant of the composites is effectively increased.[23] This phenomenon is more obvious when the content of graphene is relatively high. In addition, the layer-by-layer aligned graphene and CCTO NWs avoid contact between the fillers in the direction perpendicular to the electric field, hinder the formation of conductive paths, and inhibit the dielectric loss to a certain extent.

To explore the effect of uniaxial hot stretching on the crystal form of the composite materials, an XRD test was performed on the materials. PVDF is a semicrystalline thermoplastic fluoropolymer with five different crystalline phases (α phase, β phase, γ phase, δ phase, and ε phase); among them, the β phase is of great interest because of its polar crystalline-electroactive nature. It can be seen from Figure 5 that the

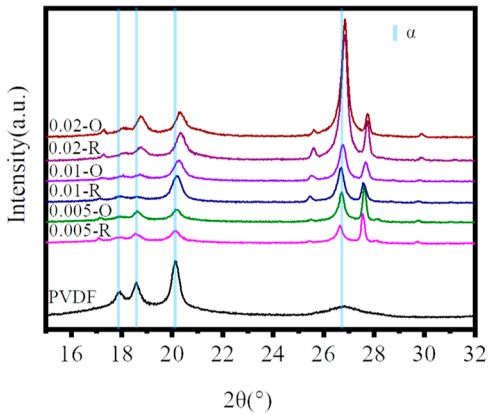

Figure 5. XRD images of the (0.2CCTO NWs−$y$graphene)/PVDF composites (y = 0.005, 0.01, and 0.02) before and after thermal stretching.

characteristic peaks of the PVDF observed at 2θ = 17.8, 18.6, 20.1, and 26.7° are strong and sharp, indicating that the crystal form in pure PVDF mainly exists in the α phase. Since the α crystal phase is nonpolar and paraelectric and the β crystal phase is ferroelectric, the β crystal phase in the PVDF crystal structure has an important influence on the dielectric properties of the PVDF composites. In order to explore whether there is β phase in the ternary composite material, a series of (0.2CCTO NWs−$y$graphene)/PVDF composites (y = 0.005, 0.01, and 0.02) before and after thermal stretching were tested by XRD. No significant β phase was observed on the XRD pattern, which can be attributed to the fact that the β phase is usually formed during compression or stretching at temperatures far below the melting point. Therefore, it can be inferred that the significant increase in the dielectric constant of the ternary orientation composite is derived from the formation of its microscopic parallel arrangement structure, which is not caused by the change in the PVDF matrix crystal phase during the stretching process.

In order to more clearly illustrate the influence of one-dimensional orientation on the dielectric properties of composites, the electric field [Figure 6(a-1−d-1)] and electric displacement vector [Figure 6(a-2−d-2)] of binary/ternary composites with random/oriented structures were studied by finite-element simulation. Table 1 shows the average electric displacement vector of the four sample models, and the calculation was completed by COMSOL software. When only CCTO NWs were included in the composite system, the dielectric constant of CCTO NWs/PVDF-O with a one-dimensional orientation structure was slightly smaller than that of CCTO NWs/PVDF-R with a random distribution. When CCTO NWs changed from random distribution to one-dimensional orientation, the increase of interfacial polarization

https://doi.org/10.1021/acsomega.3c10111
ACS Omega 2024, 9, 13298−13305

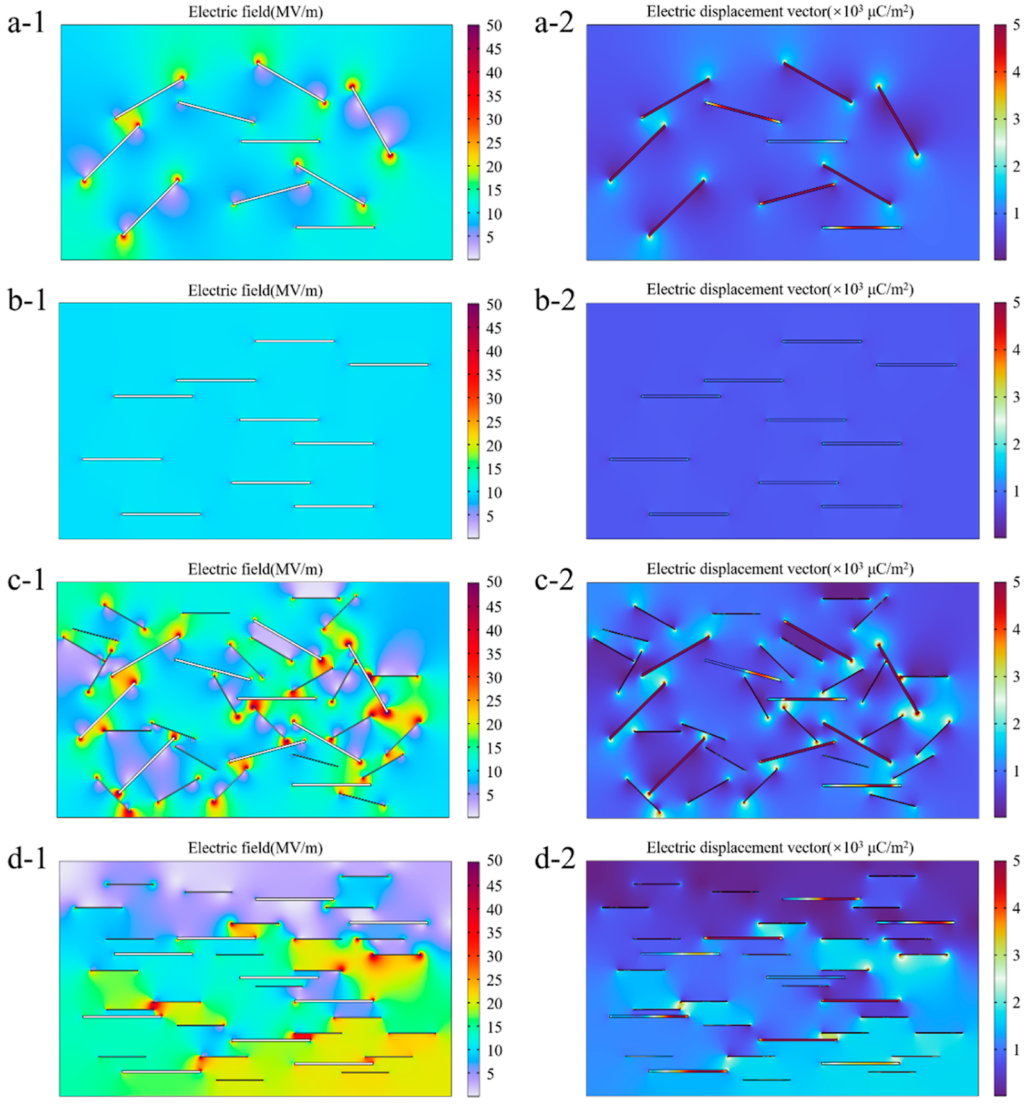

Figure 6. Two-dimensional models of binary/ternary composites with random and oriented structures were established: (a) CCTO NWs/PVDF-R composites, (b) CCTO NWs/PVDF-O composites, (c) (CCTO NWs−graphene)/PVDF-R composites, and (d) (CCTO NWs−graphene)/PVDF-O composites. Simulated distribution of (a-1−d-1) electric field and (a-2−d-2) electric displacement vector.

Table 1. Average Electric Displacement Vector (C/m^2)

sample	average electric displacement vector (C/m^2)
CCTO NWs/PVDF-R	0.8617
CCTO NWs/PVDF-O	0.8404
(CCTO NWs−graphene)/PVDF-R	0.9058
(CCTO NWs−graphene)/PVDF-O	0.9859

caused the decrease of the internal electric field of CCTO NWs, and the average electric displacement vector decreased slightly, so the dielectric constant of CCTO NWs/PVDF-O composites decreased slightly. After adding graphene as a conductive filler to composites and conducting one-dimensional orientation, the interfacial polarization between graphene and the PVDF matrix increased significantly due to the increase of the interface perpendicular to the electric field direction, thus improving the dielectric constant of the composite materials. When CCTO NWs and graphene were included in the composite system, the dielectric properties were affected by the above two factors. In the range of graphene content described in this experiment, the increase of interfacial polarization caused by graphene lamellar orientation plays a major role in improving the dielectric constant of composites. The average electric displacement vector of (CCTO NWs−graphene)/PVDF-O with significant one-dimensional orientation structure is higher than that of (CCTO NWs−graphene)/PVDF-R with a random distribution structure, so the (CCTO NWs−graphene)/PVDF-O ternary orientation composite has a higher dielectric constant. It can be seen that the electric field distortion in the composites is obvious when it is not oriented, and the one-dimensional orientation can effectively limit the degree of electric field distortion.

4. CONCLUSIONS

A strategy to obtain a high dielectric constant is demonstrated in the novel ternary (CCTO NWs−graphene)/PVDF composites, featuring the oriented CCTO NWs and graphene embedded in the PVDF matrix through a hot stretching process. Through the simultaneous introduction of conductive

https://doi.org/10.1021/acsomega.3c10111
ACS Omega 2024, 9, 13298−13305

nanofillers and high dielectric ceramic nanofillers, three-phase composites can obtain excellent dielectric properties, and their properties are far beyond pure percolation and filled polymer-based dielectric materials. At 1 kHz, the dielectric constant of the (0.2CCTO−0.02graphene)/PVDF oriented composite material is 22.33, and the dielectric loss is 0.0352. Compared with the random ternary composites, the oriented composites show a greatly increased dielectric constant, and the dielectric loss is suppressed due to the arrangement of CCTO NWs and graphene perpendicular to the electric field direction. The study demonstrates that through reasonable structural design, a balance between high dielectric constant and low loss is achieved in the case of less filler content. The results of this study may provide a feasible strategy to promote the development of high-performance polymer-based composites by adjusting the distribution of the fillers in the matrix without changing the content.

■ ASSOCIATED CONTENT

Supporting Information

The Supporting Information is available free of charge at https://pubs.acs.org/doi/10.1021/acsomega.3c10111.

SEM images and TEM image of HTO NWs; SEM images, TEM image and XRD pattern of CCTO NWs; FTIR spectra of CCTO NWs before and after 1% KH550 treatment; TEM images of graphene after peeled off for 4 h; Raman spectra of graphene; dielectric constant and dielectric loss of *x*CCTO NWs/PVDF composites (x = 0, 0.1, 0.2, 0.3, and 0.4) at 1 kHz; dielectric constant and dielectric loss of *y*graphene/PVDF composites (y = 0, 0.0025, 0.005, 0.0075, 0.01, and 0.02) at 1 kHz; dielectric constant and dielectric loss of (*x*CCTO NWs−*y*graphene)/PVDF composites (x = 0 and 0.2; y = 0, 0.0025, 0.005, 0.0075, 0.01, and 0.02) at 1 kHz (PDF)

■ AUTHOR INFORMATION

Corresponding Authors

Guang-Xin Chen − *College of Material Science and Engineering, Beijing University of Chemical Technology, Beijing 100029, PR China*; orcid.org/0000-0003-1496-361X; Email: gxchen@mail.buct.edu.cn; Fax: +86-10-64421693

Qifang Li − *Key Laboratory of Carbon Fiber and Functional Polymers, Ministry of Education, Beijing University of Chemical Technology, Beijing 100029, PR China*; orcid.org/0000-0003-0457-4784; Email: qflee@mail.buct.edu.cn; Fax: +86-10-64433585

Authors

Wenning Qi − *College of Material Science and Engineering, Beijing University of Chemical Technology, Beijing 100029, PR China*

Liuyang Li − *Key Laboratory of Carbon Fiber and Functional Polymers, Ministry of Education, Beijing University of Chemical Technology, Beijing 100029, PR China*

Ruolin Han − *College of Material Science and Engineering, Beijing University of Chemical Technology, Beijing 100029, PR China*

Yanbin Hou − *College of Material Science and Engineering, Beijing University of Chemical Technology, Beijing 100029, PR China*

Zheng Zhou − *College of Material Science and Engineering, Beijing University of Chemical Technology, Beijing 100029, PR China*

Complete contact information is available at: https://pubs.acs.org/10.1021/acsomega.3c10111

Notes

The authors declare no competing financial interest.

■ ACKNOWLEDGMENTS

The authors gratefully acknowledge the Sinopec Key Project (no. 420043) and the National Natural Science Foundation of China (no. 51573010) for providing financial support.

■ REFERENCES

(1) Luo, H.; Wang, F.; Guo, R.; Zhang, D.; He, G.; Chen, S.; Wang, Q. Progress on Polymer Dielectrics for Electrostatic Capacitors Application. *Advanced Science* **2022**, *9*, 2202438.

(2) Yang, M.; Ren, W.; Guo, M.; Shen, Y. High-Energy-Density and High Efficiency Polymer Dielectrics for High Temperature Electrostatic Energy Storage: A Review. *Small* **2022**, *18*, 2205247.

(3) Sheima, Y.; von Szczepanski, J.; Danner, P. M.; Künniger, T.; Remhof, A.; Frauenrath, H.; Opris, D. M. Transient Elastomers with High Dielectric Permittivity for Actuators, Sensors, and Beyond. *ACS Appl. Mater. Interfaces* **2022**, *14*, 40257−40265.

(4) Ma, Z.; Zhang, K.; Yang, S.; Zhang, Y.; Chen, X.; Fu, Q.; Deng, H. High-performance capacitive pressure sensors Fabricated by introducing dielectric filler and conductive filler into a porous dielectric layer through a Biomimic strategy. *Compos. Sci. Technol.* **2022**, *227*, 109595.

(5) Li, C.; Liu, J.; Lin, L.; Bai, W.; Wu, S.; Zheng, P.; Zhang, J.; Zhai, J. Superior Energy Storage Capability and Stability in Lead-Free Relaxors for Dielectric Capacitors Utilizing Nanoscale Polarization Heterogeneous Regions. *Small* **2023**, *19*, 2206662.

(6) Xia, S.; Shi, Z.; Sun, K.; Yin, P.; Dastan, D.; Liu, Y.; Cui, H.; Fan, R. Achieving remarkable energy storage enhancement in polymer dielectrics via constructing an ultrathin Coulomb blockade layer of gold nanoparticles. *Mater. Horiz.* **2023**, *10*, 2476−2486.

(7) Palani Velayuda Shanmugasundram, H. P.; Jayamani, E.; Soon, K. H. A comprehensive review on dielectric composites: Classification of dielectric composites. *Renew. Sustain. Energy Rev.* **2022**, *157*, 112075.

(8) Wang, S.; Yu, Z.; Wang, L.; Wang, Y.; Yu, D.; Wu, M. A core-shell structured barium titanate nanoparticles for the enhanced piezoelectric performance of wearable nanogenerator. *Appl. Energy* **2023**, *351*, 121835.

(9) Wang, Y.; Yao, M.; Ma, R.; Yuan, Q.; Yang, D.; Cui, B.; Ma, C.; Liu, M.; Hu, D. Design strategy of barium titanate/polyvinylidene fluoride-based nanocomposite films for high energy storage. *J. Mater. Chem. A* **2020**, *8*, 884−917.

(10) Wang, J.; Wu, H.; Wang, Z.; He, W.; Shan, C.; Fu, S.; Du, Y.; Liu, H.; Hu, C. An Ultrafast Self-Polarization Effect in Barium Titanate Filled Poly(Vinylidene Fluoride) Composite Film Enabled by Self-Charge Excitation Triboelectric Nanogenerator. *Adv. Funct. Mater.* **2022**, *32*, 2204322.

(11) Hao, X.; Liu, X.; Jiang, Y.; Wang, C.; Sun, H.; Zang, W.; Ning, N.; Tian, M.; Zhang, L. Largely improved generating energy density, efficiency, and fatigue life of DEG by designing TiO2/LNBR/SiR DE composites with a self-assembled structure. *J. Mater. Chem. A* **2022**, *10*, 9524−9534.

(12) Yu, S.; Zhang, J.; Zhu, X.; Yin, Y.; Xue, J.; Xia, F.; Li, Y.; Xue, Q. Plate-barrier architecture of rGO-TiO2 derived from MXene for constructing well-aligned polymer nanocomposites with excellent dielectric performance. *Compos. Sci. Technol.* **2022**, *218*, 109191.

(13) Zeng, Y.; Xiong, C.; Li, J.; Huang, Z.; Du, G.; Fan, Z.; Chen, N. Structural, dielectric and mechanical behaviors of (La, Nb) Co-doped

TiO2/Silicone rubber composites. *Ceram. Int.* **2021**, *47*, 22365−22372.
(14) Raghuwanshi, V.; Bharti, D.; Mahato, A. K.; Shringi, A. K.; Varun, I.; Tiwari, S. P. High Performance Flexible Organic Field-Effect Transistors with Barium Strontium Titanate Gate Dielectric Deposited at Room Temperature. *ACS Appl. Electron. Mater.* **2020**, *2*, 529−536.
(15) Su, Y.; Huan, Y.; Peng, B.; Wang, X.; Wu, L.; Wei, T. Energy storage properties of flexible dielectric composites containing Ba0.4Sr0.6TiO3/MnO2 heterostructures. *Chem. Eng. J.* **2023**, *452*, 139316.
(16) Jiang, B.; Iocozzia, J.; Zhao, L.; Zhang, H.; Harn, Y.-W.; Chen, Y.; Lin, Z. Barium titanate at the nanoscale: controlled synthesis and dielectric and ferroelectric properties. *Chem. Soc. Rev.* **2019**, *48*, 1194−1228.
(17) Shang, Y.; Feng, Y.; Zhang, C.; Zhang, T.; Lei, Q.; Chi, Q. Double gradient composite dielectric with high energy density and efficiency. *J. Mater. Chem. A* **2022**, *10*, 15183−15195.
(18) Lukacs, V. A.; Turcan, I.; Padurariu, L.; Curecheriu, L.; Cernescu, A.; Stoian, G.; Ciomaga, C. E.; Tufescu, F.; Lupu, N.; Mitoseriu, L. Nonlinear dielectric properties of BaTiO3 - Silver composites: The role of microstructure. *J. Alloys Compd.* **2020**, *817*, 153336.
(19) Santos, J. P. F.; da Silva, A. B.; Arjmand, M.; Sundararaj, U.; Bretas, R. E. S. Nanofibers of poly(vinylidene fluoride)/copper nanowire: Microstructural analysis and dielectric behavior. *Eur. Polym. J.* **2018**, *101*, 46−55.
(20) Cao, M.; Li, L.; Guo, R. Z.; Wu, S. Y.; Chen, X. M. Excellent Dielectric Properties and Finite Element Simulation of Al-Epoxy Composites with Constructed Ultrathin Al2O3 Parallel-Plate Micro-capacitors. *ACS Appl. Mater. Interfaces* **2023**, *15*, 31595−31607.
(21) Jun, S.-Y.; Park, S. H.; Sohn, M. K.; Kim, S.; Lee, J. M.; Kong, D. S.; Lee, T.-Y.; Jung, J. H.; Kim, M.-S.; Yoo, S.; Ko, J.-H.; Cha, S.; Jung, D.; Kim, J.-Y.; Yu, S. Reduction time effect on the dielectric characteristics of reduced-graphene-oxide-encapsulated barium titanate powder fillers. *Carbon* **2022**, *199*, 23−32.
(22) Liu, X.; Sun, H.; Liu, S.; Jiang, Y.; Yin, Z.; Yu, B.; Ning, N.; Tian, M.; Zhang, L. Dielectric elastomer sensor with high dielectric constant and capacitive strain sensing properties by designing polar-nonpolar fluorosilicone multiblock copolymers and introducing poly(dopamine) modified CNTs. *Composites, Part B* **2021**, *223*, 109103.
(23) Tu, H.; Wang, S.; Jiang, H.; Liang, Z.; Shi, D.; Shao, Y.; Shen, J.; Wu, Y.; Hao, X. Enhanced performance of supercapacitors by constructing a "mini parallel-plate capacitor" in an electrode with high dielectric constant materials. *J. Mater. Chem. A* **2020**, *8*, 16661−16668.
(24) Palsaniya, S.; Nemade, H. B.; Dasmahapatra, A. K. Hierarchical Nylon-6/reduced graphene oxide/polyaniline nanocomposites with enhanced dielectric properties for energy storage applications. *J. Energy Storage* **2020**, *32*, 101821.
(25) Yang, J.-h.; Xie, X.; He, Z.-z.; Lu, Y.; Qi, X.-d.; Wang, Y. Graphene oxide-tailored dispersion of hybrid barium titanate@polypyrrole particles and the dielectric composites. *Chem. Eng. J.* **2019**, *355*, 137−149.
(26) Yang, Q.; Li, C.; Zhou, W.; Li, Y.; Zhu, Y.; Ma, Y. High-dielectric porous CaCu3Ti4O12/reduced graphene oxide/polydimethylsiloxane foam for wearable, breathable and low crosstalk capacitive pressure sensor. *FlatChem* **2023**, *40*, 100522.
(27) Wu, W.; Liu, X.; Qiang, Z.; Yang, J.; Liu, Y.; Huai, K.; Zhang, B.; Jin, S.; Xia, Y.; Fu, K. K.; Zhang, J.; Chen, Y. Inserting insulating barriers into conductive particle channels: A new paradigm for fabricating polymer composites with high dielectric permittivity and low dielectric loss. *Compos. Sci. Technol.* **2021**, *216*, 109070.
(28) Zeng, Y.; Rao, S.; Xiong, C.; Du, G.; Fan, Z.; Chen, N. Enhanced dielectric and mechanical properties of CaCu3Ti4O12/Ti3C2Tx MXene/silicone rubber ternary composites. *Ceram. Int.* **2022**, *48*, 6116−6123.
(29) Zhang, J.; Hao, Y.; Liu, Y.; Wang, R.; Guo, L.; Cai, Z.; Bi, K. Space charge regulated high-k polymer nanocomposite with a novel sandwich structure. *Composites, Part B* **2020**, *203*, 108461.
(30) Cheng, S.; Zhou, Y.; Li, Y.; Yuan, C.; Yang, M.; Fu, J.; Hu, J.; He, J.; Li, Q. Polymer dielectrics sandwiched by medium-dielectric-constant nanoscale deposition layers for high-temperature capacitive energy storage. *Energy Storage Mater.* **2021**, *42*, 445−453.
(31) Niu, Y.; Dong, J.; He, Y.; Xu, X.; Li, S.; Wu, K.; Wang, Q.; Wang, H. Significantly enhancing the discharge efficiency of sandwich-structured polymer dielectrics at elevated temperature by building carrier blocking interface. *Nano Energy* **2022**, *97*, 107215.
(32) Son, J.; Lee, S.; Bae, G. Y.; Lee, G.; Duduta, M.; Cho, K. Skin-Mountable Vibrotactile Stimulator Based on Laterally Multilayered Dielectric Elastomer Actuators. *Adv. Funct. Mater.* **2023**, *33*, 2213589.
(33) Jiang, J.; Shen, Z.; Qian, J.; Dan, Z.; Guo, M.; He, Y.; Lin, Y.; Nan, C.-W.; Chen, L.; Shen, Y. Synergy of micro-/mesoscopic interfaces in multilayered polymer nanocomposites induces ultrahigh energy density for capacitive energy storage. *Nano Energy* **2019**, *62*, 220−229.
(34) Zhu, Y.; Shen, Z.; Li, Y.; Chai, B.; Chen, J.; Jiang, P.; Huang, X. High Conduction Band Inorganic Layers for Distinct Enhancement of Electrical Energy Storage in Polymer Nanocomposites. *Nano-Micro Lett.* **2022**, *14*, 151.
(35) Wu, Y.; Wang, Z.; Shen, X.; Liu, X.; Han, N. M.; Zheng, Q.; Mai, Y.-W.; Kim, J.-K. Graphene/Boron Nitride-Polyurethane Micro-laminates for Exceptional Dielectric Properties and High Energy Densities. *ACS Appl. Mater. Interfaces* **2018**, *10*, 26641−26652.
(36) Panomsuwan, G.; Manuspiya, H. Dielectric properties and discharge energy density of epoxy composites with 3D BaTiO3 network structure. *Mater. Lett.* **2020**, *270*, 127695.
(37) Tang, T.; Yang, W.; Shen, Z.; Wang, J.; Guo, M.; Xiao, Y.; Ren, W.; Ma, J.; Yu, R.; Nan, C.-W.; Shen, Y. Compressible Polymer Composites with Enhanced Dielectric Temperature Stability. *Adv. Mater.* **2023**, *35*, 2209958.
(38) You, X.; Chen, N.; Du, G. Constructing three-dimensionally interwoven structures for ceramic/polymer composites to exhibit colossal dielectric constant and high mechanical strength: CaCu3-Ti4O12/epoxy as an example. *Composites, Part A* **2018**, *105*, 214−222.
(39) Song, S.; Wang, Y.; Luo, Y.; He, D.; Abella, A.; Deng, Y. One-dimensional oriented microcapacitors in ternary polymer nanocomposites: Toward high breakdown strength and suppressed loss. *Mater. Des.* **2018**, *140*, 114−122.
(40) Feng, Y.; Wu, Q.; Deng, Q.; Peng, C.; Hu, J.; Xu, Z. High dielectric and breakdown properties obtained in a PVDF based nanocomposite with sandwich structure at high temperature via all-2D design. *J. Mater. Chem. C* **2019**, *7*, 6744−6751.
(41) Liu, Y.; Li, L.; Guo, M.; Zhou, Z.; Chen, G.-x.; Li, Q. Improving Dielectric and Mechanical Properties of CaCu3Ti4O12 Nanowire/Epoxy Composites through a Surface-Polymerized Hyperbranched Macromolecule. *ACS Appl. Electron. Mater.* **2019**, *1*, 346−353.
(42) Liu, Y.; Han, R.; Li, L.; Zhou, Z.; Chen, G.; Li, Q. Tuning of Highly Dielectric Calcium Copper Titanate Nanowires To Enhance the Output Performance of a Triboelectric Nanogenerator. *ACS Appl. Electron. Mater.* **2020**, *2*, 1709−1715.
(43) Zhang, Y.; Zhang, C.; Feng, Y.; Zhang, T.; Chen, Q.; Chi, Q.; Liu, L.; Li, G.; Cui, Y.; Wang, X.; Dang, Z.; Lei, Q. Excellent energy storage performance and thermal property of polymer-based composite induced by multifunctional one-dimensional nanofibers oriented in-plane direction. *Nano Energy* **2019**, *56*, 138−150.

https://doi.org/10.1021/acsomega.3c10111
ACS Omega 2024, 9, 13298−13305